Nuclear Clusters as a Probe for Expansion Flow in Heavy Ion Reactions at 10-15AGeV

R. Mattiello [1,2]
H. Sorge [2]
H. Stöcker [3], and W. Greiner [3]
[1] Physics Department, Brookhaven National Laboratory
Upton, New York 11973
[2] Physics Department, S.U.N.Y. at Stony Brook
Stony Brook, NY 11974
[3] Institut für Theoretische Physik, J.W. Goethe Universität
D-60054 Frankfurt am Main, Germany

January 19, 2006

Abstract

A phase space coalescence description based on the Wigner--function method for cluster formation in relativistic nucleus-nucleus collisions is presented. The momentum distributions of nuclear clusters d,t and He are predicted for central Au(11.6AGeV)Au and Si(14.6AGeV)Si reactions in the framework of the RQMD transport approach. Transverse expansion leads to a strong shoulder-arm shape and different inverse slope parameters in the transverse spectra of nuclear clusters deviating markedly from thermal distributions. A clear "bounce-off" event shape is seen: the averaged transverse flow velocities in the reaction plane are for clusters larger than for protons. The cluster yields –particularly at low p_t at midrapidities– and the in-plane (anti)flow of clusters and pions change if suitably strong baryon potential interactions are included. This allows to study the transient pressure at high density via the event shape analysis of nucleons, nucleon clusters and other hadrons.

1 Introduction

One of the challenges of modern heavy ion physics is the extraction of the equation of state and transport properties of extremely dense and excited nuclear matter. In particular, the study of matter at high net baryon density

has received much attention recently. QCD - as the accepted theory of strong interaction - contains chiral symmetry (in the limit of massless quarks) which is spontaneously broken in its ground state, the QCD vacuum (see e.g. lattice calculations [1]). A rapid restoration of this symmetry with increasing baryon density is predicted by all approaches which embody this fundamental aspect of QCD [2, 3]. Nucleus-nucleus collisions in the bombarding energy region of baryon stopping may therefore be favourable to study such medium effects as compared to ultrahigh energies, for which the two colliding nuclei may become transparent. Beam energies between 10 to 15 AGeV – as studied experimentally at the BNL-AGS [4]-[8] – seem to be well suited to stop two heavy ingoing nuclei and to create the desired high baryon densities. This has been shown by transport calculations based on hadronic excitations and rescattering like the RQMD approach (strings, resonances) [9, 10], the ARC- [12] or the ART-model [13] (resonances). The observation of stopping in the AGS experiments has been unclear for quite some time. However, all experimental groups now confirm [4]-[7] the predicted large baryon stopping in central collisions [9, 14].

An observable consequence of the formation of dense nuclear matter – far beyond the groundstate – is the emergence of collective flow driven by compression-induced pressure [15]-[18]. Mean fields [15] may give important contributions to this pressure and could therefore be accessible to experimental observation, just as in the 1GeV region [19]. The bounce-off for protons has been observed at 10 GeV/n [20] as well as azimuthally asymmetric particle correlations in the projectile hemisphere [21]. These experimental discoveries encourage us to investigate the formation of nuclear clusters – as compared to light hadrons – for which flow can even dominate the momentum spectra [17].

We follow our earlier work on deuterons [22] and extend the phase space coalescence picture to light clusters with $A \leq 4$. The basic ingredients of the cluster coalescence, i.e. the source function provided by the RQMD and the parametrization of cluster wave functions are described in Sect. 2 and 3. The parametrization of baryonic mean fields is described in Sect. 4. In Sect. 5 particular features in the momentum distributions of nuclear clusters are discussed as signatures for flow and event shape correlations at the hadronic freeze-out. In order to demonstrate sensitivities to baryonic mean fields final observables – rapidity distributions, m_t-spectra, directed flow $p_x(y)$– are compared for two extreme scenarios: one with a density-dependent quasi-potential between baryons, and the other without (cascade).

It should be mentioned that results for cluster yields have been calculated based on the thermal model and on the single-nucleon momentum distributions [23, 24, 25, 26, 27, 28, 29, 30, 31, 32, 33]. These results predict that the spectra of clusters and nucleons have essentially the same shape. Here, we are going to demonstrate that flow invalidates the basic assumptions underlying these simple models. In turn, we can use the amount of 'scaling violation' of cluster spectra as compared to proton spectra to assess the strength of collective flow in nucleus-nucleus reactions.

2 Coalescence of Clusters in Phase Space

We combine a dynamical description of the first violent stage in nucleus-nucleus reactions from the RQMD model with a cluster formation model which is based on the single-particle phase space distributions at freeze-out. RQMD is a semi-classical transport theoretical approach and does not take into account formation of nuclear bound states (e.g. deuterons) dynamically. However, the small binding energies and the associated quantum mechanical formation time from the uncertainty principle suggest that nuclear clusters are produced mainly much later after the violent interactions have ceased (freeze-out), i.e. cluster formation rates can be calculated from the nucleon distributions at freeze-out. In order to calculate light nuclear cluster distributions (for A$\leq$4) we use the Wigner-function technique in phase space. This phase space coalescence approach was already applied to deuteron production at bombarding energies around 1AGeV [34, 35], 10-15AGeV [22, 36, 37] and 160-200AGeV [38].

The validity of the combined RQMD+coalescence approach for the cluster formation clearly depends on that the transport model describes the dynamical evolution up to the freeze-out stage reasonably well. The relativistic quantum molecular dynamics approach (RQMD 1.07) [9] employed for the calculations presented here combines the classical propagation of particles with excitation of hadrons into resonances and strings. Secondaries (emerging from the decaying resonances and strings) undergo subsequent interactions, both with each other and with the ingoing baryons. Note that the RQMD-results compare well with experimental single particle and 2-body correlation data [5, 7, 10, 11].

In the following, we use the non-relativistic Wigner-function formalism which may be justified for nuclear clusters in view of the small binding energies. The formation rates are calculated at equal time in the common rest frame of the corresponding cluster nucleons immediately after their freeze-out. Having this in mind, we suppress the explicit time dependence and reference to the chosen Lorentz frame in all following expressions. Note, however, that all results presented in this work include an implicit integration over all freeze-out times and Lorentz transformations back into the original observer system.

The Wigner-function for a single particle

$$\int d^3y < \vec{x} + \vec{y}/2|\Psi >< \Psi|\vec{x} - \vec{y}/2 > e^{-\frac{i}{\hbar}\vec{p}\cdot\vec{y}} \tag{1}$$

is the closest analogue to a probabilistic distribution in phase space which one can get from quantum mechanics. Therefore, its identification with the phase space distribution $f_N \approx \rho^W$ has been frequently employed in semi-classical calculations. Neglecting the hopefully small effects from binding energies, the formation probability for a cluster can be expressed as an overlap integral between the Wigner-function which corresponds to the cluster wave function and the N-body nucleon phase space distribution at freeze-out [39, 34, 35, 22, 36, 38]. The N-body phase space distribution has to be constructed from the single par-

ticle "source function" which is defined by the "freeze-out" positions x_i^μ and momenta p_i^μ of nucleons after their last scattering or decay.

The Wigner-density of an M-nucleon state has the form

$$[\hat{\rho}_M]^W = \sum_{[TT_3]\times[SS_3]} (|SS_3><SS_3|) \times (|TT_3<TT_3|) \times W_{[TT_3]\times[SS_3]}(x_1,p_1;...,x_M,p_M) \quad (2)$$

with the normalization $\mathrm{tr}[\hat{\rho}_M] = 1$. The product $[TT_3] \times [SS_3]$ denotes the set of all 2^{2M} possible internal couplings with proper total isospin T, T_3 and spin S, S_3. Note that the phase space part $W_{[TT_3]\times[SS_3]}$ has to provide the correct symmetry concerning particle exchange to ensure that all states are totally antisymmetric. In the semiclassical approximation it is assumed that the Wigner-function does not contain *dynamical* correlations with respect to spin and isospin. We therefore employ the statistical assumption and assign all many-nucleon states which are allowed from the Pauli principle the same weight for a given position and momentum distribution:

We consider only spin averaged Wigner-densities $W_{[TT_3]\times[SS_3]} \approx 1/2^M \tilde{W}_{[T,T_3]}$. Furthermore, the coupling of M particles to a given total isospin T is assumed to be equal

$$W_{[TT_3]\times[SS_3]} \approx \frac{1}{\binom{M}{Z}} \frac{1}{2^M} \bar{W}_{T_3} = g\, \bar{W}_{T_3} \quad (3)$$

In this approach $\bar{W}_{T_3}$ contains all spin states and all $\binom{M}{Z}$ states in different isospin-multiplets for a M-particle combination (M, Z) with given charge $Z = T_3 + M/2$.

In order to approximate $\bar{W}_{T_3}$ we use the RQMD model that provides the phase space distribution of nucleons with given isospin. We identify $\bar{W}_{T_3}$ with the product of single particle distributions

$$\bar{W}_{T_3} \approx \frac{1}{N^M} \binom{M}{Z} \left[\prod_{i=1}^{Z} (2\pi\hbar)^3 f_p(\vec{x}_i,\vec{p}_i)\right] \times \left[\prod_{i=Z+1}^{M} (2\pi\hbar)^3 f_n(\vec{x}_i,\vec{p}_i)\right] \quad (4)$$

where $N = N_p + N_n$ is the total number of nucleons and

$$N_p := \int d^3x d^3p\; f_p(\vec{x},\vec{p}) \quad , \quad N_n := \int d^3x d^3p\; f_n(\vec{x},\vec{p}) \quad (5)$$

Eq. 4 can be interpreted as a statistically uncorrelated emission. It defines the probability-density to find a given nucleon combination (M,Z) in certain phase space regions. Inserted in Eq. 3 it fulfills by construction the trace normalization $\mathrm{tr}[\hat{\rho}_M] = 1$.

The cluster wave function which is assumed to be non-relativistically here factorizes into a collective and a relative part

$$|\Psi_C(\vec{P})> = \frac{1}{(2\pi\hbar)^{3/2}} e^{\frac{i}{\hbar}\vec{P}\cdot\vec{X}} \phi(\vec{t}_1,...,\vec{t}_{M-1}) |SS_3> |TT_3> \quad (6)$$

where $\vec{X} = (\vec{x}_1 + ... + \vec{x}_M)/M$ and $\vec{P} = \vec{p}_1 + ... + \vec{p}_M$. The $\vec{t}_i(\vec{x}_1, ..., \vec{x}_M)$ (i=1,...,M-1) are the $M-1$ relative coordinates of the relative cluster wave function ϕ. S, S_3, T, T_3 are the spin and isospin quantum numbers of the cluster state. The Wigner-density of the wave function in relative coordinates is defined by the Wigner-transformed projection operator

$$\hat{\rho}_C^W(\vec{t}_1, \vec{q}_1; ...; \vec{t}_{M-1}, \vec{q}_{M-1}) := \quad |TT_3 > |SS_3 > \rho_C^W < SS_3| < TT_3| \tag{7}$$

with

$$\begin{aligned} \rho_C^W \quad := \quad & \int \phi(\vec{t}_1 + \vec{y}_1/2, ..., \vec{t}_{M-1} + \vec{y}_{M-1}/2)\phi^*(\vec{t}_1 - \vec{y}_1/2, ..., \vec{t}_{M-1} - \vec{y}_{M-1}/2) \\ & \times e^{-\frac{i}{\hbar}\vec{q}_1 \cdot \vec{y}_1} \; ... \; e^{-\frac{i}{\hbar}\vec{q}_{M-1} \cdot \vec{y}_{M-1}} d^3y_1 \; ... \; d^3y_{M-1} \end{aligned} \tag{8}$$

The formation of cluster states is finally determined by the trace over the source density $\hat{\rho}_M$ and the projector on the individual cluster wave function $|\Psi_C^M >< \Psi_C^M|$:

$$\begin{aligned} \mathrm{tr}\{\hat{\rho}_M |\Psi_C^M >< \Psi_C^M|\} \quad = \quad & \int [\hat{\rho}_M]^W(\vec{x}_1, \vec{p}_1; ...; \vec{x}_M, \vec{p}_M) \hat{\rho}_C^W(\vec{t}_1, \vec{q}_1; ...; \vec{t}_{M-1}, \vec{q}_{M-1}) \\ & \times \delta^3(\vec{P} - (\vec{p}_1 + ... + \vec{p}_M)) \frac{dx_1^3 d^3p_1}{(2\pi\hbar)^3} ... \frac{d^3x_M dp_M^3}{(2\pi\hbar)^3} \end{aligned} \tag{9}$$

The absolute number of states is obtained by multiplying Eq. 9 with the total number of M-nucleon states $\binom{N}{M}$ and summation over all possible spin states N_S. Inserting Eq. 2 and 8 the semi-classical coalescence formula reads finally

$$\begin{aligned} \frac{dN}{d^3P} \quad = \quad & g N_S \binom{N}{M} \binom{M}{Z} \frac{1}{N^M} \int dx_1^3 dp_1^3 ... dx_M^3 dp_M^3 \delta^3(\vec{P} - (\vec{p}_1 + ... + \vec{p}_M)) \\ & \times \left[\prod_{i=1}^{Z} f_p(\vec{x}_i, \vec{p}_i) \right] \left[\prod_{i=Z+1}^{M} f_n(\vec{x}_i, \vec{p}_i) \right] \rho_C^W(\vec{t}_1, \vec{q}_1; ...; \vec{t}_{M-1}, \vec{q}_{M-1}) \end{aligned} \tag{10}$$

For d, t, ^{3}He and ^{4}He states the momentum distributions are explicitly given by

$$\begin{aligned} \frac{dN(d)}{d^3P} \quad = \quad & g(\mathrm{d})\; N_S(\mathrm{d}) \binom{N}{2} \binom{2}{1} \\ & \times \frac{1}{N^2} \int dx_1^3 dp_1^3 dx_2^3 dp_2^3 f_n(\vec{x}_1, \vec{p}_1) f_p(\vec{x}_2, \vec{p}_2) \\ & \times \rho_D^W \; \delta\left(\vec{P} - (\vec{p}_1 + \vec{p}_2)\right) \\ \frac{dN(\mathrm{t})}{d^3P} \quad = \quad & g(t)\; N_S(\mathrm{t}) \binom{N}{3} \binom{3}{1} \end{aligned} \tag{11}$$

$$\times \frac{1}{N^3} \int dx_1^3 dp_1^3 ... dx_3^3 dp_3^3 f_n(\vec{x}_1, \vec{p}_1) f_n(\vec{x}_2, \vec{p}_2) f_p(\vec{x}_3, \vec{p}_3)$$
$$\times \rho_t^W \; \delta\left(\vec{P} - (\vec{p}_1 + \vec{p}_2 + \vec{p}_3)\right) \tag{12}$$

$$\frac{dN(^3\mathrm{He})}{d^3P} = g(^3\mathrm{He}) \; N_S(^3\mathrm{He}) \binom{N}{3} \binom{3}{2}$$
$$\times \frac{1}{N^3} \int dx_1^3 dp_1 ... dx_3^3 dp_3^3 f_n(\vec{x}_1, \vec{p}_1) f_p(\vec{x}_2, \vec{p}_2) f_p(\vec{x}_3, \vec{p}_3)$$
$$\times \rho_{^3\mathrm{He}}^W \; \delta\left(\vec{P} - (\vec{p}_1 + \vec{p}_2 + \vec{p}_3)\right) \tag{13}$$

$$\frac{dN(^4\mathrm{He})}{d^3P} = g(^4\mathrm{He}) \; N_S(^4\mathrm{He}) \binom{N}{4} \binom{4}{2}$$
$$\times \frac{1}{N^4} \int dx_1^3 dp_1^3 ... dx_4^3 dp_4^3 f_n(\vec{x}_1, \vec{p}_1) f_n(\vec{x}_2, \vec{p}_2) f_p(\vec{x}_3, \vec{p}_3) f_p(\vec{x}_4, \vec{p}_4)$$
$$\times \rho_{^4\mathrm{He}}^W \; \delta\left(\vec{P} - (\vec{p}_1 + \vec{p}_2 + \vec{p}_3 + \vec{p}_4)\right) \tag{14}$$

In a Monte Carlo formulation – appropriate for the application to microscopic transport calculations – these formation rates can be expressed by the general coalescence formula for M-body cluster

$$dN_M = gN_S \left\langle \sum_{\substack{i_1,...,i_M \\ i_1<...<i_M}} \rho_C^W(\vec{t}_{i_1}, \vec{q}_{i_1}; ...; \vec{t}_{i_{M-1}}, \vec{q}_{i_{M-1}})) \right\rangle$$
$$\times d^3t_{i_1} d^3q_{i_1} ... d^3t_{i_{M-1}} d^3q_{i_{M-1}} \quad . \tag{15}$$

$< ... >$ denotes event averaging. The sum runs for each event over all M-nucleon combinations. Note the necessary condition $i_1 < ... < i_M$ which prevents the double counting of equal particle pairs. The coordinates in position and momentum space are taken at equal time in the M-nucleon rest frame (i.e. $\vec{P} \equiv \vec{0}$) immediately after all cluster nucleons have frozen out. The calculated numbers contain higher mass fragments by construction. The number of A$>$ 4 clusters is small, however, for rapidity values $|y - y_{mid}| < 1$. The factor g contains spin and isospin projection as described above. After the summation over all possible spin states the statistical corections are $g(\mathrm{d})N_S(\mathrm{d}) = 3/8$, $g(\mathrm{t})N_S(\mathrm{t}) = g(^3\mathrm{He})N_S(^3\mathrm{He}) = 1/12$ and $g(^4\mathrm{He})N_S(^4\mathrm{He}) = 1/96$. Feed down effects from the production of excited t and He states are expected to be small ($< 15\%$, [41]) and will be neglected in the present studies.

The statistical approximation employed here is expected to break down in regions where the binding energies and the quantum dynamics play an essential role, e.g. in case of spectator matter fragmentation. Deviations from the statistical limit could give further insight into the fermionic (quantum) dynamics of the many-body system and final state effects like e.g. Coulomb distortion.

3 The Parametrization of Cluster Wave Functions

For the deuteron we assume a Hulthén-wave function derived from a Yukawa-type potential interaction [42, 43]

$$\begin{aligned} < \vec{x}_1, \vec{x}_2 | D > &= \frac{1}{(2\pi\hbar)^{3/2}} \exp\left(\frac{i}{\hbar}\vec{P}\cdot\frac{\vec{x}_1+\vec{x}_2}{2}\right) \times \frac{4ab(a-b)}{(a+b)^2} \\ &\times \frac{1}{|\vec{x}_1-\vec{x}_2|}[\exp(-a|\vec{x}_1-\vec{x}_2|) - \exp(-b|\vec{x}_1-\vec{x}_2|)]. \quad (16) \end{aligned}$$

In order to get a simple expression for the Hulthén Wigner-density the wave function is approximated by a sum over 15 centrally symmetric Gaussian wave packets

$$\Psi(\vec{r}) = \sum_i a_i G(\vec{r}) = \sum_i a_i \left(\frac{2c_i}{\pi}\right)^{3/4} \exp(-c_i r^2). \quad (17)$$

The Wigner-density of this sum can be calculated analytically [44, 45]

$$\begin{aligned} \rho_D(\vec{r},\vec{q}) &= 8\sum_i a_i^2 \exp(-2c_i r^2)\exp\left(\frac{q^2}{2c_i}\right) \\ &+16\sum_{i>j} a_i a_j \left(\frac{4c_i c_j}{(c_i+c_j)^2}\right)^{3/4} \\ &\times \exp\left(\frac{4c_i c_j}{c_i+c_j} r^2\right) \exp\left(\frac{-q^2}{c_i+c_j}\right) \cos\left(2\frac{c_i-c_j}{c_i+c_j} rq\cos\theta_{rq}\right) \quad (18) \end{aligned}$$

with $q = |\vec{p}_1 - \vec{p}_2|/2 \quad , \quad r = |\vec{x}_1 - \vec{x}_2|$ as the relative position and momentum coordinates.

For triton, ^{3}He and ^{4}He states we use 3- and 4-particle harmonic oscillators with different coupling strength. Such an approximation has been used already in momentum coalescence studies [24, 27, 28, 29] and is well known in nuclear structure physics (see e.g. [46]). We adopt such a form of the wave function because of the separability in collective and relative motion even on the level of M-particle states. Moreover, a harmonic M-particle wave function can always be written as a product of single particle oscillators which leads to a Wigner density of the form

$$\varrho = \delta(\vec{q}_M - (\vec{q}_1 + ... + \vec{q}_{M-1})) \prod_{j=1}^{M-1} 8\, e^{-|\vec{t}_j|^2/(x_j^0)^2}\, e^{-|\vec{q}_j|^2\,(x_j^0)^2} \quad (19)$$

The $\vec{t}_j = \sum_i (\hat{C})_{ji}\vec{x}_i$ are given by the linear transformation of the original cartesian coordinates $\hat{C}$. The generalized relative momenta are $\vec{q}_j = \sum_k \left(C^{-1,+}\right)_{jk} \vec{p}_k$.

For complicated systems the transformation $\hat{C}$ can contain particle masses and different coupling constants. Our purpose has been a simple parametrization rather than taking into account detailed information in the wave function as e.g. Coulomb repulsion. Therefore, we use only one coupling constant D for each cluster and an equal mass of protons and neutrons m which leads to a representation in so-called Jacobi coordinates: For t and ^{3}He states the two relative coordinates are $\vec{t}_1 = \sqrt{3D/2}(\vec{x}_2 - \vec{x}_1)$, $\vec{t}_2 = \sqrt{2D}(\vec{x}_3 - (\vec{x}_1 + \vec{x}_2)/2)$ and $x_0^1 = x_0^2 = (3D/2m)^{1/4}$ while for ^{4}He states $\vec{t}_1 = \sqrt{2D}(\vec{x}_2 - \vec{x}_1)$, $\vec{t}_2 = \sqrt{8D/3}(\vec{x}_3 - (\vec{x}_1 + \vec{x}_2)/2)$, $\vec{t}_3 = \sqrt{3D}(\vec{x}_4 - (\vec{x}_1 + \vec{x}_2 + \vec{x}_3)/3)$ and $x_0^1 = x_0^2 = x_0^3 = (2D/m)^{1/4}$. The coupling constants are adjusted to the mean square charge radii of the diverse cluster states (see Table 1 and [47, 48, 49])

4 Baryonic Mean Fields

At nuclear ground state density the nuclear mean field may be decomposed into two large pieces: an attractive scalar field provided by the quark condensate and/or correlated two-pion exchange (the σ field), and a repulsive vector potential (the ω field) [50] which is in accord with Dirac phenomenology for optical potential calculations [51]-[54] in p+A studies and QCD sum-rule estimates [3]. Not much is known about the strength of the mean fields at large net baryon densities and temperatures predicted in all present transport approachs for the ultrarelativistic regime. It is expected that the momentum dependence [35, 51], the excitation into resonances [55] and the transition to quark matter [56] will play a crucial role for the created mean fields. Several new ideas are currently under active investigation: Medium properties of hadrons (e.g. of the ω meson which is responsible for vector repulsion [2]) or quark and gluon condensates, which break the approximate scale and chiral symmetry of the QCD Lagrangian in the vacuum, could modify the scalar field essentially [56, 3].

In the following we demonstrate the sensitivity of flow observables to mean fields by comparing two schematic cases: In the first case the potentials are switched off (i.e. the *cascade mode* is used). The second scenario uses potential type interactions which define effective baryon masses in a medium [9]

$$p_i^2 - m_i^2 - V_i = 0 \tag{20}$$

and thus simulate the effect of mean fields. Here

$$(2m_N)^{-1} V_i = +\frac{1}{2} \sum_{j,j\neq i} \alpha_{ij} \left(\frac{\rho_{ij}}{\rho_0}\right) + \frac{\beta}{\gamma+1} \left[\sum_{j,j\neq i} \left(\frac{\rho_{ij}}{\rho_0}\right)\right]^{\gamma} \tag{21}$$

with ρ_{ij} a Gaussian of the CMS distance vector normalized to one, ρ_0 ground state matter density and $\alpha = -0.4356$GeV, $\beta = 0.385$GeV, $\gamma = 7/6$ parameters which are adjusted to the saturation properties of nuclear matter (binding energy and compressibility). The parameter fit was done by taking the expectation

value of the total energy per nucleon for ideal gas (plane) wave-functions taking into account antisymmetrization. A Hamiltonian can be constructed which conserves the effective mass shell constraints of Eq. 20 [9] and is employed for the dynamical evolution in RQMD. For the presented calculations we have chosen to let the particles interact at equal times in the global equal-speed system of projectile and target.

As has been stated in [57], the experimental data for nucleus-nucleus reactions at 10-15AGeV indicate more repulsion than just given by a pure density dependence as in Eq. (3). In fact, it was found that the quasi-potentials do not affect the final distributions at all, if their strength is below a 'critical threshold'. This additional repulsion is probably caused by the momentum dependence of nuclear forces. In order to explore the possible role of mean fields, in Ref. [57] we hardened the density dependence of the potentials until we achieved agreement with experimental proton spectra which were available at that time. The attractive 2-body force in the $\Delta\Delta$ and NB^* channel have been switched off – $\alpha_{\Delta\Delta} = \alpha_{\mathrm{NB}^*} = 0$ – (thus explaining the index pair (ij) in Eq. (3)). Here, we use the same potentials. We note that this approach has predictive power for the cluster spectra, because the strength of the potentials and thus the amount of flow has been fixed from the proton spectra alone.

What does the existence of a 'critical threshold' above of which only the collective forces 'win' against the randomization of the motion by stochastic collisions and decays mean? It indicates that the mean field effect cannot be isolated from the other – stochastic – interactions which are present in the system. For instance, the initial baryon density is essentially fixed solely from the stochastic interactions, because the degree of energy degradation which the ingoing nucleons experience is mostly determined by the multiple collisions with nucleons from the other ingoing nucleus and with secondaries. More recent versions of RQMD contain somewhat more realistic interactions than used here for the presented calculations (see Ref. [58] for a discussion). For instance, the assumption of istropic heavy baryon resonance decay leads to an overestimation of the nuclear stopping power as it was noted recently in Ref. [58]. A detailed study of the interplay between the effect of collisions and mean fields based on RQMD is currently undertaken by one of us [59]. On the other side, we do not expect that our qualitative conclusions about the effect of mean fields on cluster flow will be reversed by more realistic calculations. In fact, a smaller initial baryon density means that the mean fields have to get stronger to achieve the same amount of collective flow.

5 Results and Discussion

The production of clusters has recently been measured and analyzed for central and peripheral reactions p+A, Si+A and Au+Au at AGS-energies [60, 61, 4, 62] and S+A at 200AGeV [63]. Comparisons between coalescence calculations for

deuterons at $p_t = 0$ and measurements for pA reactions have also been discussed in [60, 36]. We will first show that the phase space coalescence in combination with the RQMD freeze-out describes absolute values and momentum distributions of deuterons in accordance with measurements for various nucleus-nucleus collisions. In Fig. 1 we compare our recently published results for deuterons in central Si+A reactions at 14.6AGeV [22] with E802 data [61]. In Fig. 2 calculations for transverse mass spectra of protons and deuterons in the reaction Au(11.6AGeV)Au (b<3fm) at rapidity $y = 1.3$ are compared to preliminary E866-data [64] for central events. A comparison between calculations and data requires proper event selection according to experimental trigger conditions and acceptance corrections for the theoretical calculations [65]. On the level of the systematic errors in the measurements ($\approx 15\%$, [65, 61]), however, we find good agreement – even for the strong slope parameter splitting between protons and deuterons in massive reactions.

5.1 Transverse Expansion and Cluster Flow

The formation of transverse blast waves was first proposed in Ref. [66] where pion and proton transverse momentum spectra around 1AGeV incident beam energy were analyzed. The most prominent observables are the characteristic shoulder-arm shape and different apparent temperatures for particles with different mass. These are caused by the overlay of rather small local momenta and collective motion which have been produced during the expansion phase of the reaction. Several investigations followed in the low energy regime [17, 16, 67, 68] as well as for ultrarelativistic nucleus-nucleus reactions [69, 70, 71, 72, 22, 38].

In the following we will discuss the momentum spectra of nuclear clusters which show a strong dependence on such phase space correlations. In particular heavy clusters like ^{4}He can serve as a very promising tool to determine the phase space picture as e.g. provided by the microscopic transport calculations. The strongest flow and mean field effects are achieved in central reactions Au(11.6AGeV)Au. Variations with the reaction size and life time of the high density zone are studied by comparison with results for Si+Si reactions at 14.6AGeV. All results presented here have been calculated for central impact parameters (Au+Au: b<3fm, Si+Si: b<1fm). The weak decay of hadrons after the freeze-out has been suppressed.

Rapidity distributions and transverse momentum spectra of p, d, t and ^{4}He cluster are shown in Figs. 3 and 4 for central Au+Au (11.6AGeV) and Si+Si (14.6AGeV) reactions. The figures contain cascade (solid histograms) and potential calculations (bold solid histograms). The solid lines in Fig. 4 show Boltzmann distributions with temperature parameters adjusted to fit the transverse spectra for p_t >2GeV/c (Au+Au) and p_t >1GeV/c (Si+Si) as calculated with baryon potential-interaction.

In Au+Au collisions all rapidity distributions peak at midrapidity indicating strong stopping in accordance with earlier predictions and preliminary data for

protons [14, 22]. The transverse distributions have a strong shoulder-arm shape which deviates markedly from distributions expected from a purely thermalized fireball. The shoulder-arm shape becomes most prominent for heavy clusters. For ^{4}He clusters a peak even appears at finite p_t. The high momentum tail of the transverse spectra exhibit different 'apparent' temperatures for clusters with different mass while a thermal system would predict similar slope parameters [31]. Note that the extracted temperature values depend strongly on the p_t-cut choosen. The absolute values extracted by exponential parametrizations always lead to additional systematic errors in the absolute yields according to our calculation overestimating the cluster yields substantially. Therefore, comparisons of rapidity distributions between calculations and extrapolated data must be done very carefully.

In contrast, all rapidity distributions are essentially flat for the light system Si+Si. The transverse spectra are in good agreement with a thermal fit and show temperature parameters which are almost equal for all states.

The characteristic deviations from thermal distributions are caused by strong transverse expansion and collective flow particularly in massive reactions like Au+Au. The flow-correlations at the microscopic freeze-out are shown in Fig. 5 which contains calculations for the freeze-out velocities and density profiles of protons, deuterons, tritons and ^{4}He. The velocity profiles for all clusters are similar. They exhibit a convex shape and saturate at $\approx$0.7c for both reactions. In the massive system Au+Au the freeze-out densities have a complicated shape which peakes around 5fm. Most of the nucleons freeze out at larger distance. This is indicated by an average freeze-out radius of $\approx$ 10fm (see Table 2). The strong transverse expansion in Au+Au collisions is caused by the considerable baryon stopping and the pile up of high particle densities near to the reaction center. During the expansion phase comoving particles undergo frequent collisions transporting the system collectively sidewards until the flow-induced pressure pushes them into the vacuum. Hence, the suppression of particle emission at $r_t \rightarrow 0$ is basically caused by the dynamical expansion: many nucleons are transported through the medium before they reach the 'surface' and freeze out. Table 2 gives the average values for freeze-out radii, collective flow velocities and transverse momenta of particles in the central rapidity region. Note that the average transverse 'velocities' $< p_t > /A$, the transverse flow velocities and source radii decrease with increasing A and saturate for cluster masses $A \geq 3$. The relative suppression of cluster formation at the 'surface' ($r_t >$ 6fm) contradicts the present fireball analyses which assume a common density and velocity profile for all particles.

Clusters are clearly dominated by the collective flow components in the final phase space distribution: The collective transverse velocities of heavier mass clusters already provide most of the total transverse momentum ($\approx$80%). Therefore, the freeze-out density and collective velocity profiles determine the final spectra almost exclusively:

It is convenient to approximate the collective velocity profile by β_t=$A(r_t$ –

$r_0)^B$ in order to demonstrate the effect of the interwining of collective velocities and freeze-out probabilities on the transverse spectra. This parametrization leads to a transverse momentum spectrum of the form

$$\frac{\mathrm{d}N}{p_t \mathrm{d}p_t} = \frac{m_0^2}{BA^{2/B}} \frac{(m_t^2 - m_0^2)^{(1-B)/B}}{(m_t^2)^{(1+B)/B}} \rho(r_t) \quad ; \quad m_t := \sqrt{m_0^2 + p_t^2} \qquad (22)$$

where ρ=$1/(r_t - r_0)\mathrm{d}N/\mathrm{d}r_t$. The only quantities which determine such a purely flow-induced spectrum are the shape of the velocity profile defined by the parameter B and the density distribution ρ. Assuming a box density profile the spectra have a convex shape and maximum at finite p_t only for $B<1$ – consistent with the RQMD results. A quadratic r_t-dependence (B=2) would instead yield an overall concave spectrum, in particular diverging at $p_t \to 0$.

The flattening of the transverse spectra at low p_t-values is due to the suppression of clusters in the very central region of the reaction ($r_t \to 0$). The different apparent temperatures at high p_t-values are caused by the strong weight of large flow velocities for $r_t > 6$fm. The peak/shoulder in the transverse spectra, however, appears approximately at $p_t/A \approx < \beta_t >$ and directly measures the strength of the transverse flow at the position where most of the clusters at central rapidities freeze out ($r_t \approx 5 - 7$fm). Note that it is not possible to describe the transverse spectra with one single temperature and collective flow velocity in contrast to what has been claimed for reactions in the 1GeV/n regime [67, 68].

Si+Si collisions do not provide a transverse expansion comparable to massive reactions (Fig. 5, Table 2). Most of the clusters are emitted close to the beam axis where the transverse flow velocities are small. In fact, the 'surface suppression' acts more strongly in the case of the smaller system, in accordance with the larger surface to volume ratio. Note that here the average transverse flow velocity of ^{4}He states is approximately a factor of two smaller than for protons (Table 2). Transverse flow is nearly invisible due to large 'local' momentum components. This sampling of clusters at smaller distances from the beam axis explains why the transverse flow features are mostly invisible, although the velocity profiles for cluster states in Fig. 5 – the 'collective' position-momentum correlations – are almost equal for Si+Si and Au+Au collisions.

The role of the shapes of collective velocity and density profiles has been the subject of much previous debate [17, 22, 67, 69, 70, 68]. In particular the low-p_t pion enhancement and the spectra of protons and deuterons have been interpreted in terms of transverse flow with the assumption of an expanding thermal fireball [69, 70]. A similar picture has been used to extract 'local temperatures' and chemical potentials exploiting the final particle ratios [71, 72]. We wish to discuss this issue in more detail because in those analyses the freeze-out profiles used differ significantly from the results of the transport calculations presented here.

In Ref. [69] a value for $B = 2$ in combination with a box-shaped density profile was used to explain the low-pt pion enhancement i.e. a concavely curved

p_t-spectrum. As a consequence of these assumptions proton and deuteron spectra show the same behaviour, in particular for $p_t \to 0$. The microscopic calculation, however, contradicts this picture and shows profiles which are compatible with $B \approx 0.5$ and a non-trivial position geometry. The concave curvature of transverse spectra in the transport calculations has been confirmed by recent data (see protons and deuterons in Si+A reactions at 14.6AGeV [61] and the results for Au(11.6AGeV)Au in Fig. 2). In this sense, neither the assumption $\rho = const$ nor a shape of the freeze-out profile according to $B = 2$ –as used in [69]– can be justified. The main reason for the misleading results in [69] is probably the misinterpretation of concavely shaped pion spectra. Pions are strongly influenced by the final decays of resonances such as Δ, ρ, B^* (see [73] and Refs. therein). The alternative prediction that the low-p_t pion excess at AGS energy comes from Δ-resonances [74, 10] has been confirmed by experimental reconstruction of the pπ invariant masses which show a strong Δ-signal, in agreement with RQMD [7]. Furthermore, the early preliminary data for protons used in [69] were limited in acceptance ($m_t - m_0 > 200$MeV). They excluded those regions where most of the shoulder-arm effect appears and were – within the error bars – also consistent with concavely shaped distributions for protons and deuterons.

5.2 Directed Flow

Besides the characteristic signals in the inclusive spectra, the correlation between rapidity and directed transverse momentum $p_x(y)$ in Fig. 6 is another indicator of a non-trivial event geometry. This observable is well known as the nuclear "bounce-off" discovered first at the Bevalac [75]. The averaged transverse velocity p_x/A in Fig. 6 is defined by the averaged transverse momentum per cluster nucleon projected on the theoretical reaction plane for particles within a certain rapidity interval Δy:

$$p_x(y_0)/A := \left\langle \frac{1}{N} \sum_i \hat{e}_x \cdot \vec{p}_i/A \right\rangle \Bigg|_{|y-y_0|<\Delta y/2} \tag{23}$$

$\hat{e}_x$ is the unity vector which points perpendicular to the beam axis into the impact parameter plane. $\langle ... \rangle$ denotes the final event averaging. In the case of strong longitudinal and transverse flow contributions in the final source this quantity reflects the collective sideward flow of matter predicted by hydrodynamics [15, 76] and microscopic models [15, 14, 76].

Clusters exhibit larger $p_x(y)/A$ values than nucleons although the division by A excludes the trivial effect of the momentum scaling with mass $p_A/A \simeq p_N$ at equal velocity. This stronger correlation for cluster states is well known from Au+Au reactions in the 1GeV/n energy regime [77, 19]. The reason for this behaviour is demonstrated in Fig. 7 which shows profiles for the collective in-plane velocity $\beta_x = \hat{e}_x \cdot \vec{p}/E$ and freeze-out density of protons and deuterons.

Only particles in the forward hemisphere $2.1 < y < 2.6$ are taken into account. The profiles are drawn as a function of the transverse distance to the beam axis taken in the original nucleon-nucleon cms and projected onto the theoretical reaction plane $x := \vec{x} \cdot \hat{e}_x$.

The densities for deuterons are scaled by an arbitrary factor to exhibit the qualitative difference between nucleons and deuterons: In contrast to the average values, the 'local' velocities of protons and deuterons are equal. The density distribution of the deuterons, however, exhibits a shift towards the outward regions as compared to protons. This suppression of cluster formation near to the original beam axis is caused by higher relative momenta for nucleons. Therefore, the high transverse in-plane velocities are more strongly weighted in the case of cluster formation which leads to higher *average* velocities. Note the qualitative difference between this increase in the reaction plane in contrast to decreasing values for $< p_t >$ /A at central rapidities.

5.3 Mean Field Dependences

The results in calculations for Au+Au show higher longitudinal (Fig. 3) and transverse momenta (Fig. 4, Table 2) caused by the additional pressure which is built up by the repulsive mean fields at high baryon density (up to $8\rho_0$ is achieved [14]). Note that the region of highest compression (ρ/ρ_0>3) is large (V$\simeq$several hundred fm^3) and contains up to 60% baryons in resonance states [73].

The difference between potential and cascade calculations is largest in the low-p_t part of the spectra (Fig. 4). For heavier clusters the distributions close to $p_t = 0$ change by up to a factor of three. Nuclear matter at midrapidities is mostly affected by the mean field contributions at high baryon densities: Figs. 8 and 9 show the rapidity dependence of the proton and deuteron yields at low transverse momenta – here defined by a cut in transverse momentum $p_t/A < 0.5$GeV – and the average transverse momenta of p, d and ^{4}He. While cascade calculations exhibit a clear peak in the dN/dy spectra, the calculations including potentials show a dip even for central events. This is due to the additional longitudinal expansion caused by the baryon potential interaction. The potentials also change the average transverse momenta by <20%.

For the smaller system Si+Si the average transverse momenta change by less than 3% including potential-interaction. In earlier work we have shown that the life time of the reaction is not long enough to establish a thermalized high density phase [14]. The 'transverse communication' is in light systems much smaller and does not allow for a considerable transverse push due to the mean fields, although, potentials also lead to qualitative changes in the distribution of the longitudinal momenta for the small system: The results in Fig. 3 show that cascade calculations exhibit a concave shaped spectrum which turns to a convex distribution if potentials are included. As in Au+Au reactions the yields of cluster states are most sensitive: The dN/dy values for ^{4}He states at

midrapidity differ by almost a factor of 2 between the cascade and the potential calculations.

The value of the flow-correlation $p_x(y)$ in central Au(11.6AGeV)Au collisions is roughly a factor 1.5-2 higher due to the additional sideward push of the mean fields (Fig. 6). In recent work we have shown that pions and other produced hadrons (antikaons, antinucleons) show a characteristic 'anti-flow' [78] caused by scattering off spectator-like matter. This behaviour has previously been discussed in reactions at 1AGeV [79, 80, 68]. Fig. 6 includes this pionic anti-flow which also appears to be sensitive to the baryonic mean fields, too: While cascade calculations show sizeable p_x/m values for πs, the inclusion of baryonic potentials leads to almost vanishing $p_x(y)$-values in the laboratory frame. In the principal axis system, however, the strong anticorrelation of pions to baryons is conserved. In the work of Li et al. [81] the in-plane pion flow has been investigated in the framework of the cascade model ART. In these calculations the sign of the pionic flow is equal to the baryon flow in central events which is in qualitative difference to the RQMD results. Note the strong dependence of the in-plane pion flow on different absorption rates at high baryon densities which has recently been analyzed for reactions at lower incident beam energies with the QMD-model [80].

Both results for central Au(11.6AGeV)Au collisions including baryon potentials (high in-plane flow for nucleons, small p_x/m for pions) are in quantitative agreement with preliminary flow measurements from E877 [82] and E866. The convex proton rapidity distribution in Si+Si and the width of the distribution in Au+Au reactions, including potential interactions, are also in accord with published [61] and preliminary [4, 22] data. Nevertheless, even potential calculations overestimate stopping and underestimate the transverse momentum production at forward rapidities ($y > y_{NN}$) in asymmetric reactions like Si+Au [65]. The results for deuterons in Fig. 1 show the same trend.

6 Summary and Outlook

We have presented a phase space coalescence model for cluster formation with $A \geq 2$ in relativistic nucleus-nucleus collisions using the Wigner-function method. The combination with the transport approach RQMD allows the calculation of cluster momentum distributions. Specifically, we have studied central Au(11.6-AGeV)+Au and Si(14.6AGeV)+A reactions. The microscopic model shows that strong stopping results in observable collective behaviour of the stopped baryon-rich matter. Considerable flow ($< \beta > \approx 0.5$ c) develops due to the internal pressure of the dense matter. The transverse expansion is most visible in the momentum spectra of nuclear clusters which deviate markedly from thermal distributions. In central Au(11.6AGeV)Au collisions the transverse spectra exhibit a strong shoulder-arm shape which is most prominent for heavier mass clusters.

The 'apparent' temperatures at high transverse momenta, which result from the overlay of rather small local momentum fluctuations and collective flow velocities, increase with cluster mass. Furthermore, a clear "bounce-off" event shape is seen in massive reactions like Au(11.6AGeV)Au. The averaged transverse flow velocities in the reaction plane $< p_x > (y)/A$ are markedly larger for clusters than for protons (by a factor of 2). Both the shoulder-arm shape and the large bounce-off signal for nuclear clusters are directly related to the freeze-out geometry and flow correlations. In contrast to the directed flow our results show smaller freeze-out radii and smaller average transverse 'velocities' $< p_t > /A$ for clusters at midrapidities than for free protons. This result is in contradiction to simple fireball and blast wave models.

The cluster spectra and the in-plane flow may change markedly if baryon potential-interactions are included: According to the calculations presented here the yields of nuclear clusters decrease by up to a factor of three, at low p_t and central rapidities, in the reaction Au(11.6AGeV)Au. The average p_t/A values are ≈15% harder in calculations with potentials than in the cascade mode. The $p_x(y)$-correlation for nucleons and nuclear clusters increases by a factor of 1.5-2 while the anticorrelated in-plane flow of pions vanishes. For central Si(14.6AGeV)Si reactions the potentials play a negligible role in transverse direction, but affect the proton and cluster rapidity spectra. Cascade calculations exhibit concave spectra which turn into convex distributions if potentials are taken into account. The absolute yield for ^{4}He clusters changes by almost a factor of two at midrapidity. The strong sensitivity of nuclear clusters to the collective flow encourage the quantitative study of the transient pressure in nucleus-nucleus collisions.

Acknowledgement

This work has been supported by the BMFT, GSI, DFG and the A.v.Humboldt-foundation. One of us (R.M.) wants to thank the nuclear theory and experimental groups at BNL and SUNY for their kind hospitality and useful discussions.

References

[1] J.B. Kogut, D.K. Sinclair and K.C. Wang: Phys. Lett. B163(1991)101

[2] U. Vogl and W.Weise: Prog. Part. Nucl. Phys. 27(1991)195; W. Weise: Nucl. Phys. A553(1993)59

[3] X. Jin, T.D. Cohen, R.J. Furnstahl and D.K. Kriegel: Phys. Rev. C47(1993)2882 and refs. therein

[4] M. Gonin for the E802/E866 collaboration: Nucl. Phys. A566(1993),601c

[5] Hideki Hamagaki for the E-802/866 collaboration: Nucl. Phys. A566(1993),27c

[6] K.J. Foley for the E810 collaboration: Nucl. Phys. A544(1992)335c

[7] J. Stachel for the E-814/877 collaboration: Nucl.Phys. A566(1993),183c

[8] J. Barette for the E-814/877 collaboration: Nucl. Phys. A566(1993),411c

[9] H.Sorge, H. Stöcker and W. Greiner: Ann. Phys. (NY) 192(1989)266; Nucl. Phys. A498(1989)567c; H. Sorge, A. v. Keitz, R. Mattiello, H. Stöcker and W. Greiner: Z. Phys. C47 (1990)629

[10] H. Sorge, R. Mattiello, H. Stöcker and W. Greiner: Phys. Lett. B271(1991)37

[11] J.P. Sullivan, M. Berenguer, D.E. Fields, B.V. Jacak, M. Sarabura, J. Simon-Gillo, H. Sorge, H. van Hecke, S. Pratt: Phys. Rev. Lett. 70(1993)3000; Nucl. Phys. A566(1994)531c

[12] S.H. Kahana, Y. Pang and T.J. Schlagel: Nucl. Phys. A566(1993),465c and refs. therein

[13] B.A. Li, C.M. Ko: Phys. Rev. C52 (1995) 2037

[14] H. Sorge, A.v. Keitz, R. Mattiello, H. Stöcker, W. Greiner: Phys. Lett. B 243(1990)7

[15] H.Stöcker and W. Greiner: Phys. Rep. 137(1986)278; H. Kruse, B.V. Jacak, and H. Stöcker: Phys. Rev. Lett. 54(1985)289; J.J. Molitoris, J.B. Hoffer, H. Kruse and H. Stöcker: Phys. Rev. Lett. 53(1984)899; G. Buchwald, G. Graebner, J. Theis, J. Maruhn, and W. Greiner: Phys. Rev. Lett. 52(1984)1594; Ch. Hartnack, M. Berenguer, A. Jahns, A. v. Keitz, R. Mattiello, A. Rosenhauer, J. Schaffner, T. Schönfeldt, H. Sorge, L. Winckelmann, H. Stöcker, W. Greiner: Nucl. Phys. A538(1992)53c;

[16] P. Danielewicz and Q. Pan: Phys. Rev. C46(1992)2002; Q. Pan and P. Danielewicz: Phys. Rev. Lett. 70(1993)2062,3523

[17] H. Stöcker, A. Ogloblin, W. Greiner: Z. Phys. A303(1981)259; S. Nagamiya, M.-C. Lemaire, E. Moeller, S. Schnetzer, G. Shapiro, H. Steiner, and I. Tanihata: Phys. Rev. C24(1981)971

[18] J.J. Molitoris, H Stöcker, H.A. Gustafsson, J. Cugnon, D. L'Hote: Phys. Rev. C33 (1986),867

[19] K.-H. Kampert: J.Phys. G15(1989)691; H.H. Gutbrod, K.H. Kampert, B.W. Kolb, A.M. Poskanzer, H.G. Ritter and H.R. Schmidt: Phys. Lett. B216(1989)267

[20] J. Barrette for the E877 collaboration: Nucl. Phys. A590(1995)259c

[21] T. Abott for the E802 collaboration: Phys. Rev. Lett. 70(1993)1393

[22] R. Mattiello, A. Jahns, H. Sorge, H. Stöcker, W. Greiner: Phys. Rev. Lett. 74(1995)2180

[23] A. Schwarzschild and C. Zupancic : Phys. Rev. 129(1963)854

[24] H. Sato, K. Yazaki: Phys. Lett. B98(1981)153

[25] C.B. Dover, U. Heinz, E. Schnedermann, J. Zimanyi: Phys. Rev. C44 (1991)1636

[26] H. Gutbrodt, A. Sandoval, P. Johanssen, A. Poskanzer, O. Gosset, W. Meyer, G. Westfall, R. Stock: Phys. Rev. Lett. 37 (1976)667

[27] H. Bando: Nuovo Cim. 102A (1989) 627; H. Bando, M. Sano, J. Zofka and M. Wakai: Nucl. Phys. A501 (1989) 900

[28] F. Asai, H. Bando, M. Sano: Phys. Lett. 145B (1984) 19

[29] M. Wakai, H. Bando, M. Sano: Phys. Rev. C38(1988)748

[30] H. Kruse, B.V. Jacak, J.J. Molitoris, G.D. Westfall, H. Stöcker: Phys. Rev. C31(1985)1770

[31] A. Mekijan: Phys. Rev. Lett. 38(1977)640; Phys. Rev. C17(1978)1051

[32] P.R. Subramanian, L.P. Csernai, H. Stöcker, J.A. Maruhn, W. Greiner, H. Kruse: J. Phys. G: Nucl. Phys. 7(1981)L241

[33] D. Hahn und H. Stöcker: Nucl. Phys. A476(1988)718

[34] M. Gyulassy, K. Frankel and E.A. Remler: Nucl. Phys. A402(1983)596

[35] J. Aichelin, A. Rosenhauer, G. Peilert, H. Stöcker, and W. Greiner: Phys. Rev. Lett. 58(1987) 1926; J. Aichelin, E.A. Remler: Phys. Rev. C35(1987) 1291

[36] J.L. Nagle, S. Kumar, D. Kusnezov, H. Sorge, R. Mattiello: Phys. Rev. C53(1996)367

[37] M. Bleicher, C. Spieles, A. Jahns, R. Mattiello, H. Sorge, H. Stöcker, W. Greiner: Phys. Lett. B361(1995)10

[38] H. Sorge, J.L. Nagle, B.S. Kumar: Phys. Lett. B 355(1995)27

[39] E.A. Remler and A.P. Sathe: Ann. of Phys. 91(1975)295 ;E.A. Remler: Ann. of Phys. 95 (1975) 455 ; E.A. Remler: Ann. of Phys. (NY) 136(1981)293

[40] S. DeBenedetti: *Nuclear Interactions* (John Wiley 1964)

[41] D.R. Tilley, H.R. Weller, H.H. Hasan: Nucl. Phys. A474(1987)1; D.R. Tilley, H.R. Weller, G.M. Hale: Nucl. Phys. A541(1992)1

[42] R.G. Sachs and M. Goeppert-Mayer: Phys. Rev. 53(1938)991

[43] L. Hulthen: Ark. Mat. Ast. Fys. 28, No. 5

[44] P.B. Siegel and M. Farrow-Reid: Am. J. Phys. 58(1990) 1016

[45] G.R. Shin and J. Rafelski: J. Phys. G: Nucl. Part. Phys. 16(1990)L187

[46] H.J. Mang: Phys. Rev. 119 (1960) 1069

[47] R. Hofstätter: Rev. Mod. Phys. 28(1956)214

[48] J. Carlson: Phys. Rev. C38 (1988) 1879

[49] C.R. Chen, G.L. Payne, J.L. Friar, B.F. Gibson: Phys. Rev. C33 (1986)1740

[50] B.D. Serot and J.D. Walecka: Adv. Nucl. Phys. 15 (1986); J. Theis et al.: Phys. Rev. D28 (1983)2286

[51] E.D. Cooper, B.C. Clark, R. Kozack, S. Shim, S. Hama, J.I. Johansson, H.S. Sherif, R.L. Mercer, B.D. Serot: Phys. Rev. C36(1987)2170

[52] M. Jaminon, C. Mahaux, P. Rochus: Nucl. Phys. A365(1981)371

[53] B. Ter Haar and R. Malfliet: Phys. Lett. B172(1986)10

[54] T.L. Ainsworth, E. Baron, G.E. Brown, J. Cooperstein, M. Prakash: Nucl. Phys. A464(1987)740

[55] F. de Jong and R. Malfliet: Phys. Rev. C46(1992)2567

[56] J. Ellis, J. Kapusta, K. Olive: Phys. Lett. B273(1991)122

[57] H. Sorge, R. Mattiello, H. Stöcker and W. Greiner: Phys. Rev. Lett. 68(1992)286.

[58] H. Sorge: Phys. Rev. C52(1995)3291

[59] H. Sorge: manuscript in preparation

[60] J.L. Nagle, B.S. Kumar, M.J. Bennett, G.E. Diebold, J.K. Pope, H. Sorge, J.P. Sullivan: Phys. Rev. Lett. 73 (1994) 1219

[61] T. Abbott for the E802 collaboration: Phys. Rev. C50 (1994) 1024

[62] D. Beavis for the E878 collaboration: Phys. Rev. Lett. 75(1995)3078

[63] J. Gillo et al.: Nucl. Phys. A590(1995),483c

[64] Ziping Chen for the E802 collaboration: Contrib. to the First Int. Conf. on Frontiers of Physics, Shantou, China, August 1995

[65] B. Moscowitz, M. Gonin, F. Videbaek, H. Sorge, R. Mattiello: Phys. Rev. C 51(1995)310

[66] P.J. Siemens and J.O. Rasmussen: Phys. Rev. Lett. 42(1978)880

[67] M.A. Lisa for the EOS collaboration: Phys. Rev. Lett. 75(1995) 2662

[68] J. Konopka: PhD-thesis, J.W. Goethe Universität Frankfurt am Main, 1995

[69] K.S. Lee and U. Heinz: Z. Phys. C48(1990)525; K.S. Lee, U. Heinz and E. Schnedermann: Z. Phys. C48 (1990) 525

[70] E. Schnedermann and U. Heinz: Phys. Rev. Lett. 69 (1992) 2908

[71] P. Braun-Munzinger, J. Stachel, J.P. Wessels, N. Xu: Phys. Lett. B365(1996)1

[72] A.D. Panagiotou, G. Mavromanolakis, J. Tzoulis: Phys. Rev. C53(1996)1353

[73] M. Hofmann, R. Mattiello, H. Sorge, H. Stöcker and W. Greiner: Phys. Rev. C51(1995) 2095

[74] G.E. Brown, J. Stachel, G.M. Welke: Phys. Lett. B253(1991)19

[75] H.A. Gustafsson, H.H. Gutbrod, J. Harris, B.V. Jacak, K.H. Kampert, B.Kolb, A.M. Poskanzer, H.G. Ritter and H.R. Schmidt: Mod. Phys. Lett. A3(1988)1323

[76] N.S. Amelin, E.F. Staubo, L.P. Csernai, V.D. Toneev, K.K. Gudima, D. Strottman: Phys. Rev. Lett. 67(1991)1523

[77] M. D. Partlan for the EOS collaboration: Phys. Rev. Lett. 75(1995)2100

[78] A. Jahns, Chr. Spieles, H. Sorge, H. Stöcker and W. Greiner: Phys. Rev. Lett. 72(1994) 3464

[79] S.A. Bass, R. Mattiello, H. Stöcker, W. Greiner and Ch. Hartnack: Phys. Lett. B302 (1993) 381

[80] S.A. Bass, C. Hartnack, H. Stöcker, W.Greiner: Phys. Rev. C51(1995)3343

[81] B.A. Li, C.M. Ko: Phys. Rev. C53(1996)R22

[82] J. Wessels (E877-collab.): Proc 11^{th} Winter Workshop on Nuclear Dynamics, Key West, in press

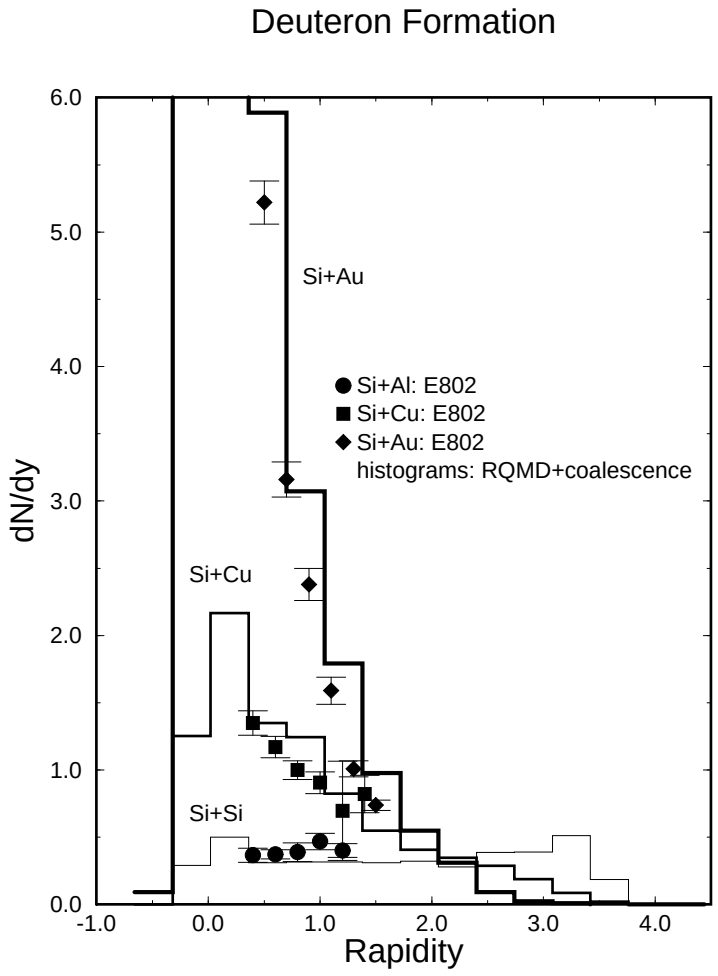

Figure 1: Rapidity distributions of deuterons in Si+Si (b< 1fm), Si+Cu (b< 1.5fm) and Si+Au (b< 3fm) reactions at 14.6AGeV calculated from RQMD simulations including potential interactions for baryons (solid histograms). The symbols show E802-data from Ref. [61] for central Si+Al, Cu and Au reactions. Note that the data have been extrapolated in m_t and contain $\approx 15\%$ systematic uncertainty.

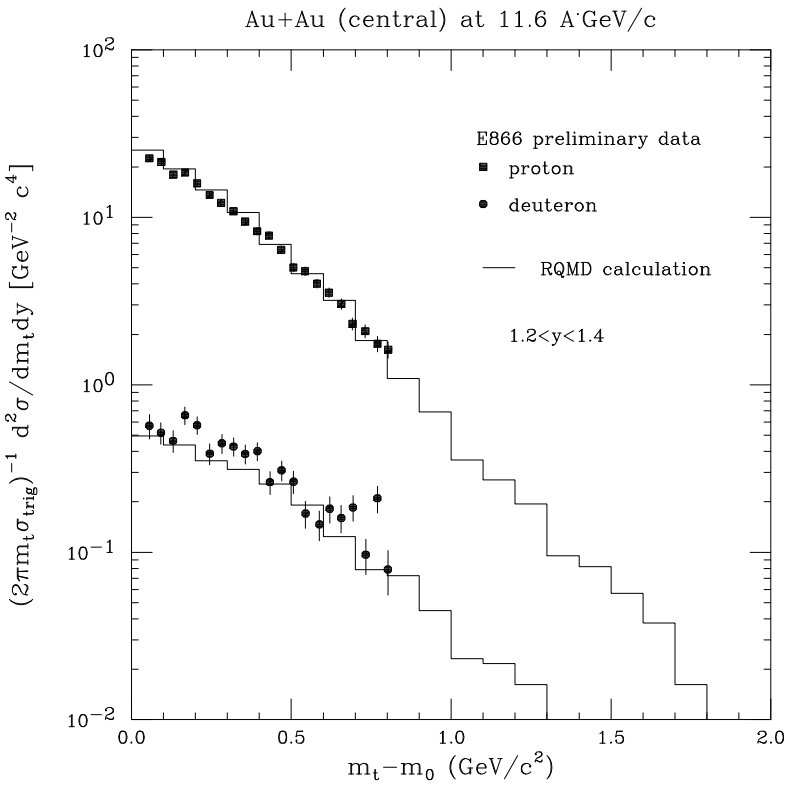

Figure 2: Transverse mass spectra for protons and deuterons in central Au(11.6AGeV)Au reactions at $y_{LAB} = 1.3$. RQMD-simulations including potential interactions for baryons (histograms) are compared with preliminary E866-data (symbols) [64].

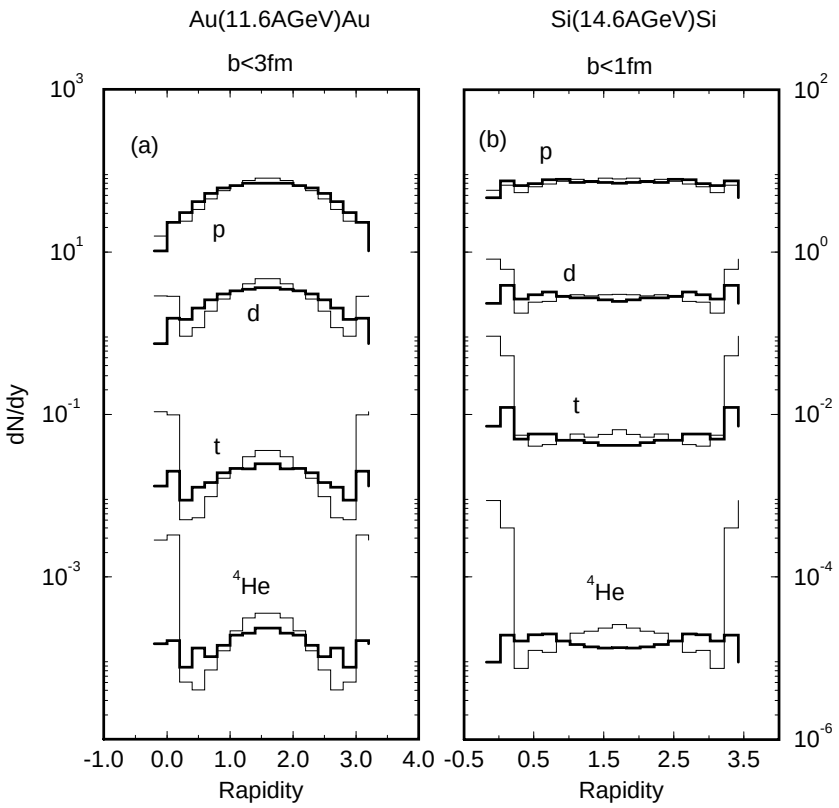

Figure 3: Rapidity distributions for p,d,t and ^{4}He in Au(11.6AGeV)Au, b< 3fm (a) and Si(14.6AGeV)Si, b< 1fm (b). Calculations with baryon potentials are denoted by bold solid histograms. Cascade calculations are shown by thin solid histograms. The inclusion of potentials at high baryon densities leads to stronger longitudinal expansion in both systems.

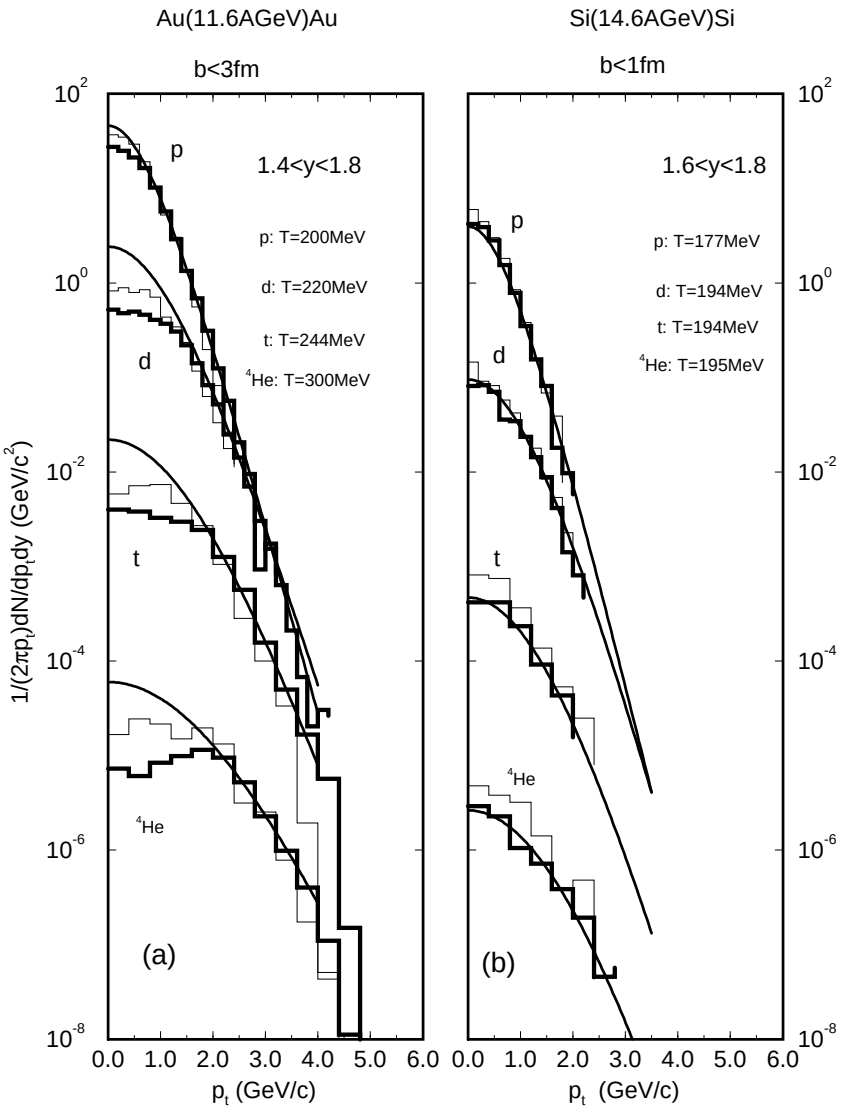

Figure 4: Transverse momemtum spectra for p,d,t and ^{4}He in Au(11.6AGeV)Au, b< 3fm (a) and Si(14.6AGeV)Si, b< 1fm (b) at central rapidities. Calculations including baryon potentials (bold solid histograms) are compared with cascade simulations (thin solid histograms). The smooth solid lines show Boltzmann parametrizations adjusted to the high momentum part of the spectra (see text) in calculations with potential interaction.

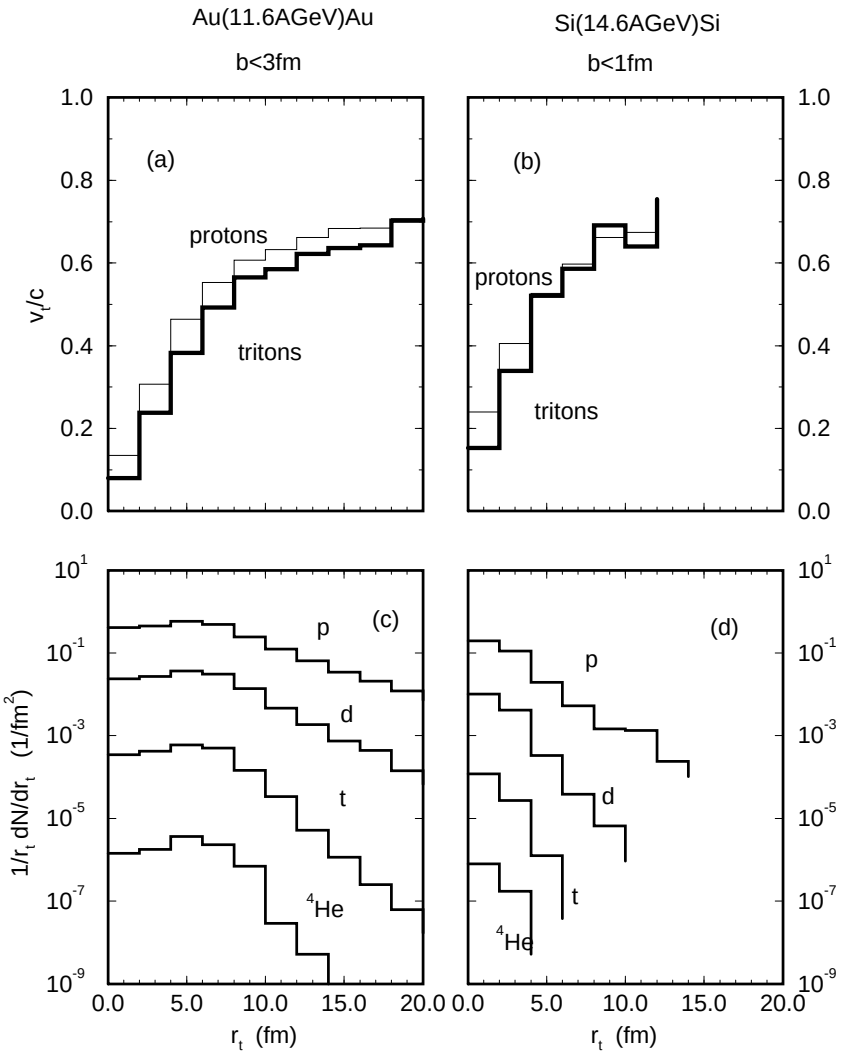

Figure 5: Freeze-out profiles of protons and tritons in RQMD-calculations including baryon potentials for Au(11.6AGeV)Au, b< 3fm (a,c) and Si(14.6AGeV)Si, b< 1fm (b,d) at central rapidities. The upper part shows transverse velocity profiles for protons and tritons. The lower part shows the distributions of transverse freeze-out densities of p, d, t and ^{4}He.

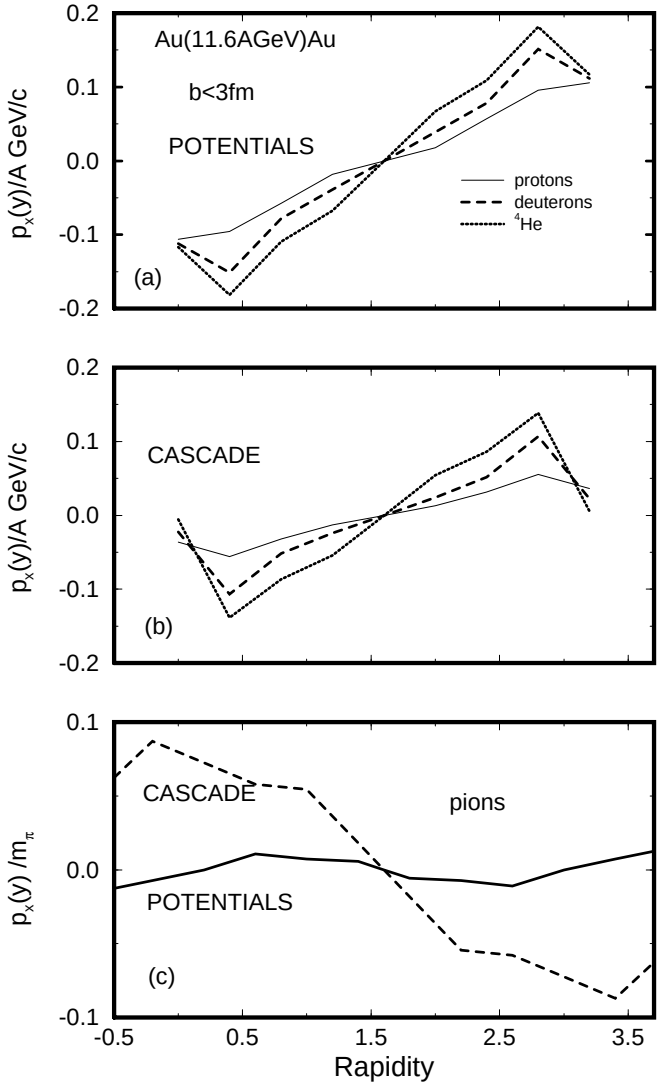

Figure 6: $p_x(y)/A$-correlations for p, d, ^{4}He (a,b) and pions (c) in central Au(11.6AGeV)Au (b< 3fm) reactions. The figure shows a factor of two increase of the cluster flow if baryon potentials are included. The additional rotation of the event plane due to the potentials leads to an apparent vanishing of the pion flow in the laboratory system which is, however, still pronounced in the principal axis system of the rotated (baryon) event.

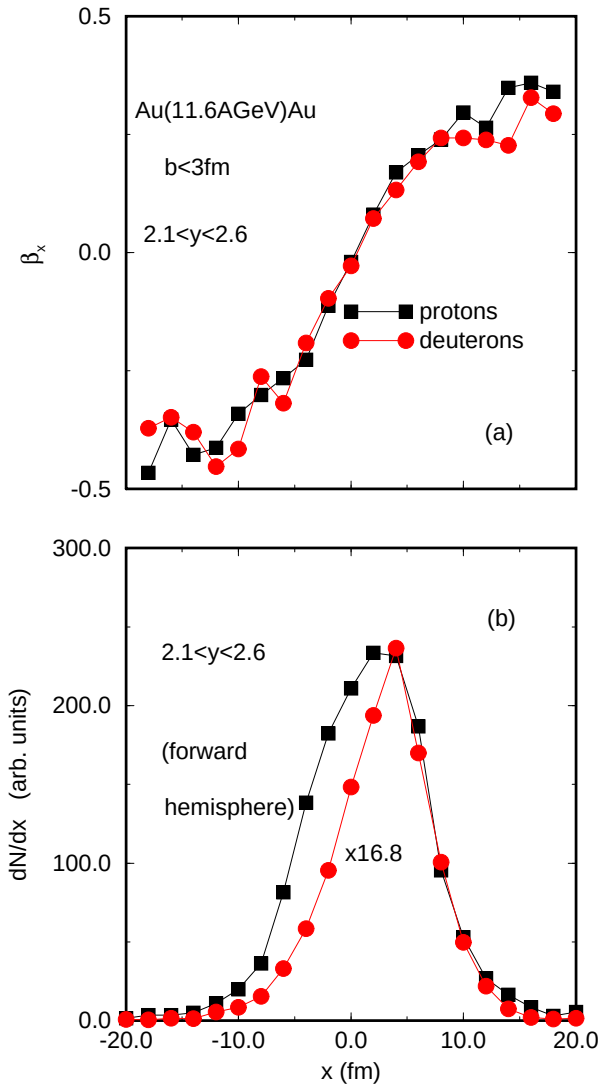

Figure 7: In-plane freeze-out velocity (a) and density profiles (b) of protons and deuterons in central Au(11.6AGeV)Au reactions (b< 3fm). Selected are particles in the forward ($2.1 < y_{\rm Lab} < 2.6$) hemisphere. x denotes the projection of the freeze-out position onto the theoretical reaction plane. The deuteron density is scaled by a factor 16.8 to demonstrate the increase in the transverse freeze-out distances from the beam axis between protons to deuterons.

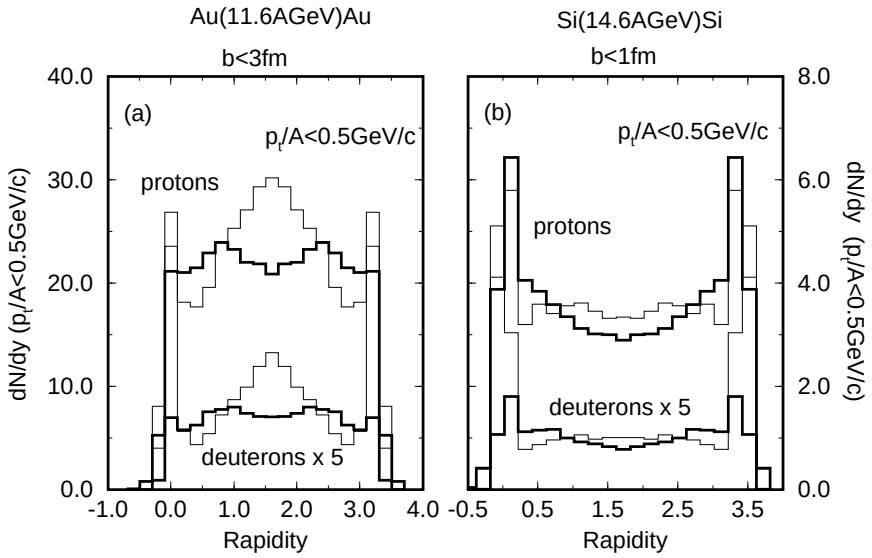

Figure 8: Comparison of dN/dy-distributions of protons and deuterons including a transverse momentum cut $p_t/A < 0.5$AGeV in calculations with (bold solid histograms) and without baryon potentials (thin solid histograms) for central Au(11.6GeV)Au (a) and Si(14.6AGeV)Si (b) reactions.

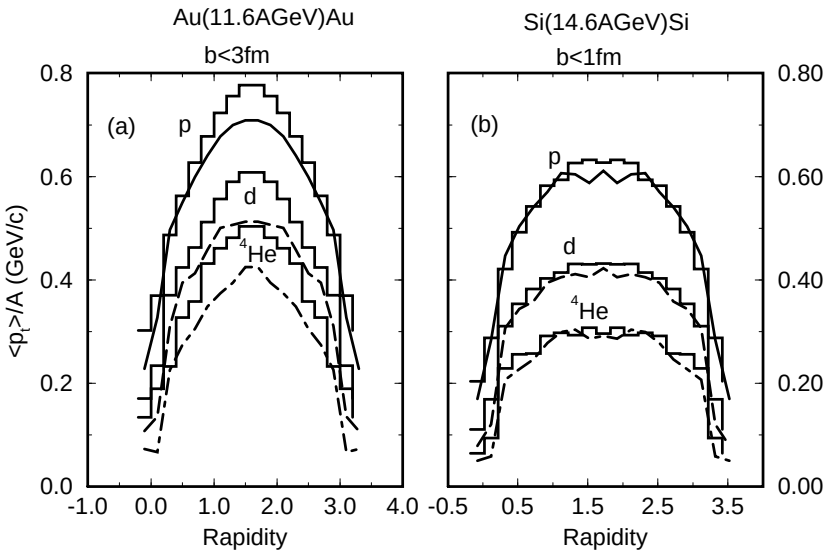

Figure 9: Average transverse momenta $< p_t > (y)$ of p, d, ^{4}He in calculations with (histograms) and without (lines) baryon potentials for central Au(11.6GeV)Au (a) and Si(14.6AGeV)Si (b) reactions.

Table 1		
cluster	radius (fm)	D (GeV^3)
^{3}H	1.7	0.27×10^{-4}
^{3}He	1.8	0.34×10^{-4}
^{4}He	1.5	0.53×10^{-4}

Tab. 1 Root mean square charge radii for nuclear clusters with A=3,4 and the corresponding coupling strength in the harmonic oscillator approach.

Table 2												
	n	p	d	t	^{3}He	^{4}He	n	p	d	t	^{3}He	^{4}He
Au+Au cascade							Au+Au potentials					
$<\beta_t>$	.5	.5	.42	.37	.38	.36	.54	.54	.47	.43	.44	.42
$\sqrt{<r_t^2>}$ (fm)	9.5	9.7	7.9	6.6	6.2	6.0	10.0	9.9	7.9	6.6	6.9	6.2
$<p_t>/A$(GeV/c)	0.71	0.71	0.51	0.44	0.44	0.43	0.77	0.78	0.61	0.51	0.53	0.50
Si+Si cascade							Si+Si potentials					
$<\beta_t>$	.39	.39	.32	.26	.26	.24	.41	.40	.31	.24	.26	.23
$\sqrt{<r_t^2>}$ (fm)	3.9	3.7	2.7	2.2	2.2	1.8	3.9	3.9	2.7	2.2	2.3	2.1
$<p_t>/A$ (GeV/c)	0.62	0.61	0.42	0.32	0.33	0.29	0.64	0.63	0.43	0.33	0.34	0.30

Tab. 2 Average transverse freeze-out velocities $<\beta_t>$, freeze-out radii $\sqrt{<r_t^2>}$ and average transverse momenta $<p_t>/A$ for nucleons and cluster with $A \leq 4$ in central Au(11.6AGeV)Au and Si(14.6AGeV)Si reactions. The table contains calculations with (r.h.s.) and without (l.h.s.) baryon potential-interaction. Only particles in the midrapidity region $1.4 < y < 1.8$ (Au+Au) and $1.6 < y < 1.8$ (Si+Si), respectively, are taken into account.